Validation of Local Structural Loads Computed by OpenFAST Against Measurements From the Focal Experimental Campaign

Preprint

Lucas Carmo, Roger Bergua, Lu Wang, and Amy Robertson

National Renewable Energy Laboratory

Presented at the 43rd International Conference on Ocean, Offshore and Arctic Engineering (OMAE® 2024)
Singapore
June 9-14, 2024

NREL is a national laboratory of the U.S. Department of Energy
Office of Energy Efficiency & Renewable Energy
Operated by the Alliance for Sustainable Energy, LLC

This report is available at no cost from the National Renewable Energy Laboratory (NREL) at www.nrel.gov/publications.

Contract No. DE-AC36-08GO28308

Conference Paper
NREL/CP-5000-88671
July 2024

Validation of Local Structural Loads Computed by OpenFAST Against Measurements From the Focal Experimental Campaign

Preprint

Lucas Carmo, Roger Bergua, Lu Wang, and Amy Robertson

National Renewable Energy Laboratory

Suggested Citation
Lucas Carmo, Roger Bergua, Lu Wang, and Amy Robertson. 2024. *Validation of Local Structural Loads Computed by OpenFAST Against Measurements From the Focal Experimental Campaign: Preprint*. Golden, CO: National Renewable Energy Laboratory. NREL/CP-5000-88671. https://www.nrel.gov/docs/fy24osti/88671.pdf.

NREL is a national laboratory of the U.S. Department of Energy
Office of Energy Efficiency & Renewable Energy
Operated by the Alliance for Sustainable Energy, LLC

This report is available at no cost from the National Renewable Energy Laboratory (NREL) at www.nrel.gov/publications.

Contract No. DE-AC36-08GO28308

Conference Paper
NREL/CP-5000-88671
July 2024

National Renewable Energy Laboratory
15013 Denver West Parkway
Golden, CO 80401
303-275-3000 • www.nrel.gov

NOTICE

This work was authored by the National Renewable Energy Laboratory, operated by Alliance for Sustainable Energy, LLC, for the U.S. Department of Energy (DOE) under Contract No. DE-AC36-08GO28308. Funding provided by the U.S. Department of Energy Office of Energy Efficiency and Renewable Energy Wind Energy Technologies Office. The views expressed herein do not necessarily represent the views of the DOE or the U.S. Government. The U.S. Government retains and the publisher, by accepting the article for publication, acknowledges that the U.S. Government retains a nonexclusive, paid-up, irrevocable, worldwide license to publish or reproduce the published form of this work, or allow others to do so, for U.S. Government purposes.

Cover Photos by Dennis Schroeder: (clockwise, left to right) NREL 51934, NREL 45897, NREL 42160, NREL 45891, NREL 48097, NREL 46526.

VALIDATION OF LOCAL STRUCTURAL LOADS COMPUTED BY OPENFAST AGAINST MEASUREMENTS FROM THE FOCAL EXPERIMENTAL CAMPAIGN

Lucas Carmo[1,*], Roger Bergua[1], Lu Wang[1], Amy Robertson[1]

[1]National Renewable Energy Laboratory, Golden, CO

ABSTRACT

This work presents the validation of the local structural load modeling capability in OpenFAST for floating substructures based on data from the FOCAL experimental campaign. Previously, OpenFAST could only represent the floating substructure as a rigid body, and though this approach can model the global response of the floater in most cases, it is not able to capture the structural loads within the floater's individual members. Consideration of local substructure loads is important for some floating designs, because the pursuit of cost reduction often results in lighter and more flexible structures. To address this limitation, the HydroDyn (hydrodynamics) and SubDyn (substructure dynamics) modules of OpenFAST have been recently extended to account for the flexibility of floating substructures. To validate this new capability, we compare the results obtained by OpenFAST with data measured during the FOCAL experimental campaign, which analyzed a 1:70 scale performance-matched model of the IEA 15-MW reference turbine atop a modified University of Maine VolturnUS-S semisubmersible in a wave basin under the action of both wind and waves. For the purposes of the present work, the most important feature of the experiment is the presence of load cells at the root of each pontoon, and our objective is to assess how well those loads are reproduced by OpenFAST. To model the distributed hydrodynamic and hydrostatic loads along the floating substructure, we adopt a strip-theory approach based on the Morison equation, and we discuss the impact of different hydrodynamic modeling options (wave stretching, MacCamy-Fuchs correction, and second-order wave kinematics) on both motions and loads. For simplicity, we focus on wave-only conditions, both regular and irregular. The results demonstrate good overall agreement for the loads at the root of the pontoons for the waves analyzed in this work, especially given the assumptions and simplifications inherent to a simple strip-theory model.

Keywords: Floating offshore wind turbine; Substructure flexibility; Member-level loads; Validation; OpenFAST; SubDyn; HydroDyn

*Corresponding author: lucas.carmo@nrel.gov

1. INTRODUCTION

Floating offshore wind turbines (FOWTs) are expected to play a key role in the future of wind energy, because they can harness the vast wind resource potential located in deep water areas that are not available to bottom-fixed turbines [1]. These turbines are complex structures, so their design relies heavily on numerical simulations to assess the performance and structural robustness of the system across a diverse range of environmental and operational conditions. These simulations usually involve use of aero-hydro-servo-elastic software programs, which are numerical tools that account for the nonlinear couplings between aerodynamics, hydrodynamics, controls, moorings and structure.

Among these tools, OpenFAST [2]—developed by the National Renewable Energy Laboratory—is a widely used open-source software for coupled nonlinear time-domain aero-hydro-servo-elastic simulations of both land-based and offshore wind turbines. It has been successfully used to model a wide range of fixed-bottom and floating wind turbines [3–5]. However, until recently, the software could only represent the floating substructure as a rigid body. Though this approach can model the global response of the floater in most cases, it is not able to capture the structural loads and deformations within its individual members. Consideration of local substructure loads is important for some floating designs, as the pursuit of cost reduction often results in lighter and more flexible structures.

To address this limitation, the HydroDyn (hydrodynamics) and SubDyn (substructure dynamics) modules of OpenFAST were recently extended to account for the flexibility of floating substructures [6]. An initial code-to-code verification of this capability was performed by comparing the results obtained by OpenFAST with those from the commercial software OrcaFlex for the TetraSpar FOWT [7]. The results showed good agreement for the global response of the floater, except for some discrepancies attributed to different modeling approaches.

A natural progression is to validate this new OpenFAST capability with experimental results, and this is our goal in the present work. To do so, we compare OpenFAST simulations against data measured during Campaign 4 of the Floating Offshore-wind

and Controls Advanced Laboratory (FOCAL) project [8–12]. It consisted of experiments of a 1:70 scale performance-matched model of the IEA 15-MW reference turbine [13] atop a modified University of Maine VolturnUS-S semisubmersible [14] in a wave basin under the action of both wind and waves. This experimental campaign aimed to create an accessible dataset to validate turbine controls and load-mitigation techniques in numerical models; previous works have analyzed the data pertaining to the effect of tuned mass dampers [9, 12] and turbine control strategies [12]. For the purposes of the present work, the most important feature of the experiment is the presence of load cells at the root of each pontoon. Our objective is to assess how well OpenFAST can reproduce the loads measured by those load cells.

Because our goal is to model the structural loads at the pontoons, we adopt a strip-theory approach in OpenFAST based on the Morison equation to model the distributed hydrodynamic and hydrostatic loads along the floating substructure. This approach requires the adoption of empirical added mass and drag coefficients, which we have tuned based on a combination of decay tests, numerical analysis, and results from previous work [15]. We also discuss the impact of wave stretching, MacCamy-Fuchs correction, and second-order wave kinematics—some of which are recent capabilities in OpenFAST [16]—on both motions and loads. For simplicity, we focus on wave-only conditions, one regular and two irregular.

Following an overview of the FOWT model and experimental setup in Section 2, Section 3 describes the OpenFAST model and its calibration. Section 4 presents the comparisons between the results obtained with OpenFAST and the experimental measurements, while Section 5 summarizes the main conclusions.

2. MODEL PROPERTIES AND EXPERIMENTAL SETUP

The FOCAL project consisted of four experimental campaigns that studied a 1:70 scale performance-matched model of the IEA 15-MW reference turbine atop a modified VolturnUS-S semisubmersible. All the experiments were conducted at the Harold Alfond Wind-Wave Ocean Engineering Laboratory of the Advanced Structures and Composites Center at the University of Maine. Only a brief description of the experiments is given subsequently, and the reader is referred to Refs. [8–12] for details. Figure 1 shows the FOWT model in the wave basin.

The experiments analyzed the FOWT model under several different environmental conditions, including the concurrent action of waves and wind, and included complex features such as tuned mass dampers and different turbine control strategies. In this work, we are interested in a subset of the measurements obtained during Campaign 4, namely body motions and loads at the root of the pontoons. The loads at the pontoons were measured using a six-degree-of-freedom (6-DoF) load cell whose location is illustrated in Figure 2. For simplicity, we focus on wave-only conditions. We also restrict our analysis to tests where the tuned mass dampers were fixed, thus behaving like fixed ballast.

The model was moored using three horizontal fishing lines with each line connecting the base of each of the radial columns to a spring. This approach was adopted instead of a conventional catenary mooring system to reduce experimental uncertainty and facilitate the validation of numerical models. Besides the mooring lines, the model employed a bundle of umbilical cables to power the turbine and tuned mass dampers and to connect the sensors to the data acquisition system. This cable bundle had an impact on the dynamics of the body, acting mostly as a spring in the surge and heave directions that were included in the numerical model described subsequently. The natural periods of rigid-body motion of the FOWT—with the cable bundle attached—were obtained with decay tests, and the results for the degrees of freedom considered in this work are listed in Table 1.

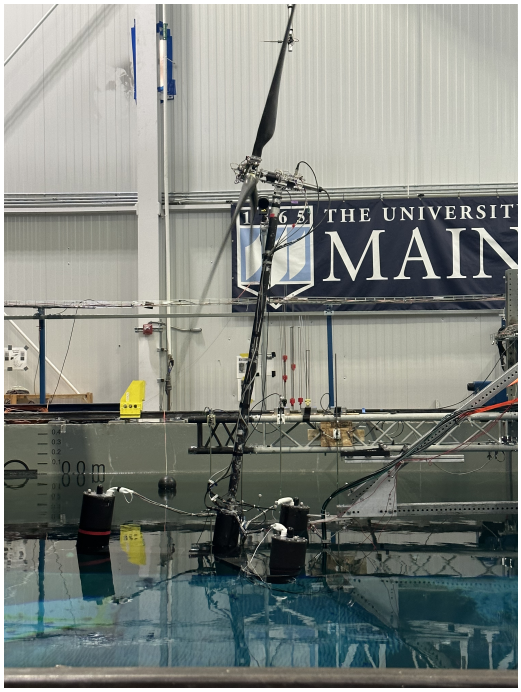

FIGURE 1: Picture of the 1:70 model of the VolturnUS-S semisubmersible in the Alfond Wind-Wave basin. Photo from the University of Maine.

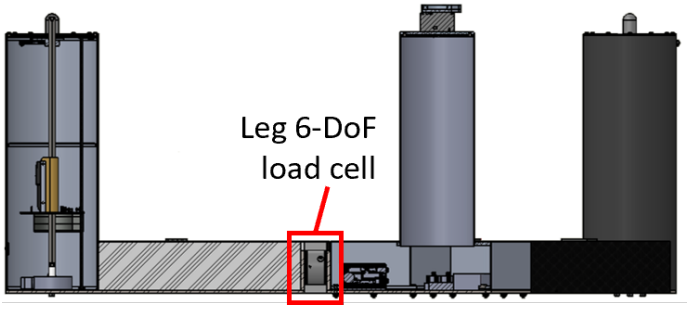

FIGURE 2: Side view of the floating substructure showing the 6-DoF load cell at the root of one of the pontoons. Illustration modified from [9].

TABLE 1: Natural periods/frequencies from decay tests

DoF	Surge	Heave	Pitch
Period (s)	80.52	20.85	30.51
Frequency (Hz)	0.012	0.048	0.033

We consider three wave conditions, one regular (REG) and two irregular (IRR01 and IRR02), with their characteristics listed in Table 2. The irregular waves correspond to the severe sea state (IRR01) and the operational sea state (IRR02) considered in previous works [8, 10–12]. The waves propagate along the X direction (incidence angle of 0°), aligned with one of the pontoons of the floating substructure.

TABLE 2: List of wave conditions considered in this work

Wave condition	Type	Peak period (s)	Significant height (m)	Peak shape
REG	Regular	13.5	10.85	-
IRR01	JONSWAP	12.7	8.18	2.75
IRR02	JONSWAP	8.9	3.20	1.80

3. NUMERICAL MODEL

We analyzed the FOWT model from FOCAL Campaign 4 using OpenFAST v4.0.0 [2]. This section described the main modeling approaches adopted in the different OpenFAST modules. We consider a coordinate system with the origin at the intersection between the mean water level and the tower axis, with the X axis aligned with the waves, the Z axis directed upwards, and the Y axis following from the right-hand rule. The numerical model was developed at full scale, and all information reported herein is also at full scale.

3.1 Structural model

We modeled the floating substructure in OpenFAST using SubDyn. Figure 3 presents an illustration of the SubDyn model, with the elements in yellow corresponding to flexible beams (2-node Timoshenko beam) and the elements in red to rigid links. Because the columns of the experimental model were very rigid, we modeled each column as a lumped mass located at its center of gravity (CoG) connected to the neighboring element by rigid links.

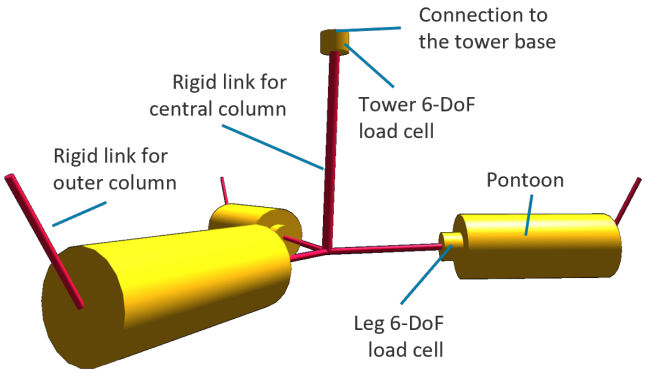

FIGURE 3: Illustration of the floating substructure modeled in SubDyn. Elements in yellow correspond to flexible beams and the ones in red to rigid links.

When we performed this study, SubDyn was only capable of modeling circular elements, thus requiring some assumptions to approximate the rectangular pontoons. We adopted the following:

- To ensure the same buoyancy as the 12.43 – m × 7.08 – m pontoon, we considered a circular pontoon with a diameter of 10.58 m. Though buoyancy is actually modeled by HydroDyn, we decided to keep the same value in both modules for consistency.
- To obtain the same cross-section moment of inertia of the rectangular pontoon with respect to the horizontal axis, we considered a thickness of $t = 1.08$ m. This approach can well model the bending in the vertical direction, which is our focus, but not the bending in the horizontal direction.
- To match the mass of the pontoons measured in the experiments, we adopted a material density of 2,704 kg/m^3.

For the 6-DoF load cells, we modeled each of them as a beam with the dimensions reported by the manufacturer, which in full scale correspond to a length of 3.09 m and a diameter of 4.58 m. They are located at a radial distance of 17.68 m from the axis of the central column. We set the density to 5,430.1 kg/m^3 to match the mass of the load cells and set the bending stiffness to $EI = 8.16 \times 10^{12}$ Nm^2 to match the first natural frequency of bending of the pontoons (about 0.80 Hz).

Table 3 summarizes the main inputs provided to SubDyn. Table 4 lists the main inertial properties obtained with SubDyn alongside the difference with respect to the experiments.

TABLE 3: Main inputs for the SubDyn model

Central column	
Mass (t)	5,352
CoG* coord. (m)	(1.14, -0.26, -17.14)†
Outer columns‡	
Mass (t)	1,244
CoG coord. 1 (m)	(25.87, -44.82, -5.21)
CoG coord. 2 (m)	(25.87, 44.82, -5.21)
CoG coord. 3 (m)	(-51.75, 0.00, -5.21)
Pontoons	
Length (m)	24.79
Diameter (m)	10.58
Thickness (m)	1.08
Density (kg/m^3)	2,703.8
Young modulus (N/m^2)	3.44×10^9
Load cells	
Length (m)	3.09
Diameter (m)	4.58
Thickness (m)	2.20
Density (kg/m^3)	5,430.1
Young modulus (N/m^2)	4.00×10^{10}

* Center of gravity.
† Eccentricity mostly due to the umbilical cable.
‡ Without the tuned mass dampers, which are included in ServoDyn.

The SubDyn model interfaces with ElastoDyn at the top of the load cell that is located at the tower base. The ElastoDyn model is responsible for solving the rigid-body motions of the platform (surge, sway, heave, roll, pitch, and yaw) and the first

fore-aft and first side-to-side bending modes of the tower. All other degrees of freedom were disabled. The inertial properties of the tower and the rotor-nacelle assembly included in ElastoDyn are the same from previous works [8–12].

TABLE 4: Main inertial properties of the floating substructure obtained with SubDyn and difference with respect to the experimental values

	Numerical model	$\frac{Y_{num} - Y_{exp}}{Y_{exp}}$
Mass	18 726 t	0.4%
Vert. center of mass from keel	7.11 m	-1.3%
Pitch/roll gyradius†	27.3 m	4.3%

† About center of mass.

3.2 Hydrodynamic model

Because our goal is to model the structural loads at the pontoons, we adopt the strip-theory approach available in HydroDyn to obtain distributed hydrodynamic and hydrostatic loads. To assess the performance of the strip-theory model, we compare to simulation results from a hybrid model that uses a combination of the quadratic drag from the Morison equation with radiation/diffraction loads obtained from frequency-dependent coefficients precomputed with WAMIT [17]—including full quadratic transfer functions (QTFs). This hybrid model comprises only one potential-flow body with the radiation/diffraction loads lumped at a single point of the structure; hence, it is only able to model the rigid-body motions of the structure. To study the internal loads at the pontoons with the hybrid approach, it would be necessary to discretize the floating substructure into multiple potential-flow bodies. This is possible with OpenFAST but not done in the present work.

Similar to SubDyn, the strip-theory approach in HydroDyn is only capable of modeling circular elements. As a workaround to model the rectangular pontoons, we use circular cylinders with a diameter of 10.58 m to ensure the same buoyancy as the rectangular pontoon and to model the loads in the horizontal direction. To account for the differences in the flow due to the different dimensions in the vertical and horizontal directions, we include five fictitious vertical cylinders within each pontoon. Those fictitious elements do not contribute to buoyancy or to the forces in the horizontal direction, being simply auxiliary elements to allow for an independent calibration of the model in the horizontal and vertical directions. The model is illustrated in Figure 4.

We consider several hydrodynamic models to evaluate the impact of different modeling capabilities available in OpenFAST. The first modeling capability is wave stretching, which allows for wave kinematics and resulting loads to be evaluated up to the instantaneous free surface. Previous works have shown that wave stretching is fundamental to properly reproduce the low-frequency response of some concepts of FOWTs [15, 18]. To assess the importance of wave stretching to properly reproduce the experiments, we have run OpenFAST models (i) without wave stretching, i.e., wave kinematics and loads are computed up to the mean sea level, (ii) with Wheeler stretching, and (iii) with vertical

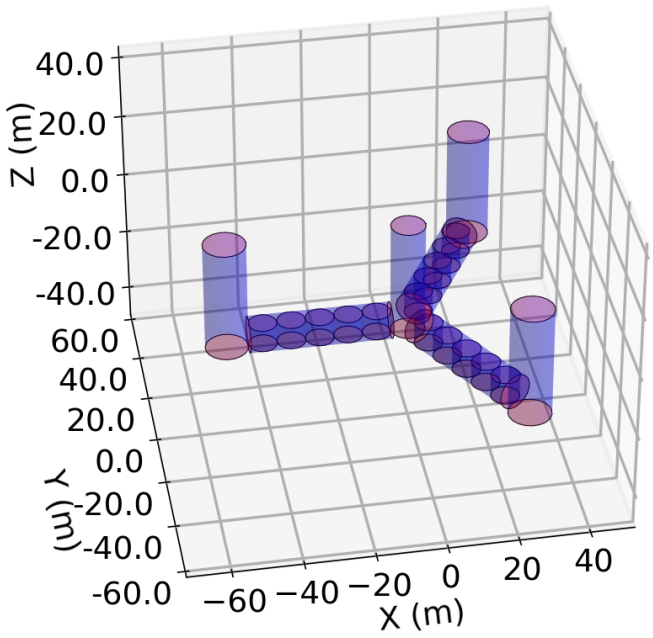

FIGURE 4: Illustration of the strip-theory model adopted in HydroDyn, including the fictitious cylinders to account for the rectangular cross-section of the pontoons

wave stretching (see [16] for details about the wave stretching models).

Another of these capabilities is the utilization of second-order wave kinematics, which allows for the inclusion of full difference-frequency and sum-frequency wave kinematics. We have run simulations with and without second-order wave kinematics to verify how that impacts the motions of, and loads on, the floating substructure. Starting in OpenFAST v4.0.0, the information related to the wave field is part of the new SeaState module.

The third aspect is the MacCamy-Fuchs correction (MCF), which is used to correct the inertial loads computed with the strip-theory approach. This correction is useful for wavelengths that are comparable to the diameter of the cylinders that comprise the body, because the inertial part of the Morison equation overestimates the wave loads in these conditions. Because the MCF is based on the analytical solution for the first-order wave loads acting on a vertical bottom-mounted surface-piercing circular cylinder [19], this correction is only applicable for elements of the floating substructure that are vertical surface-piercing circular cylinders. Moreover, as OpenFAST can evaluate wave kinematics considering the instantaneous body position, the MCF as implemented in OpenFAST acts by modifying kinematics of the incoming wave field. To reduce memory use, currently OpenFAST can only apply the MCF to vertical cylinders that have the same diameter (within 10%). Hence, in our numerical models, the MCF is applied only to the outer columns of the floating substructure.

The fourth and last hydrodynamic capability is the computation of hydrodynamic loads considering the instantaneous position of the body. For the hybrid model, which uses QTFs precom-

puted with WAMIT, the computation at the instantaneous position would lead to double counting of some second-order force components. Instead, the computation considers the low-pass filtered position of the body with a cutoff frequency of 0.04 Hz, just below the wave-frequency region to minimize double counting effects in the second-order hydrodynamic loads. This is not a problem for the strip-theory model, which considers the instantaneous body position without any problem.

The strip-theory approach requires the definition of an added-mass coefficient for the flow transversal to the cylinder axis (C_a) and an added mass coefficient for the flow that is axial to the cylinder ends ($C_{a,end}$). The first coefficient corresponds to distributed loads along the length of the cylinder, whereas the latter corresponds to lumped loads at the cylinder ends. To avoid tuning the added mass coefficients based on the experimental results, we calibrate these coefficients using the added mass and diffraction loads computed with WAMIT. We aim to obtain a set of added-mass coefficients that could match the added mass in surge, heave, and pitch at their respective natural frequencies (see Figure 5) and the wave load along the same DoFs (see Figure 6). We focus on these three DoFs because they are the only ones with significant loads and motions due to the wave incidence of 0°. The load comparisons are based on the force response amplitude operators (RAOs), which are directly output by WAMIT. For OpenFAST, we computed the load RAOs from time-domain simulations of a white-noise wave ($H_S = 2$ m).

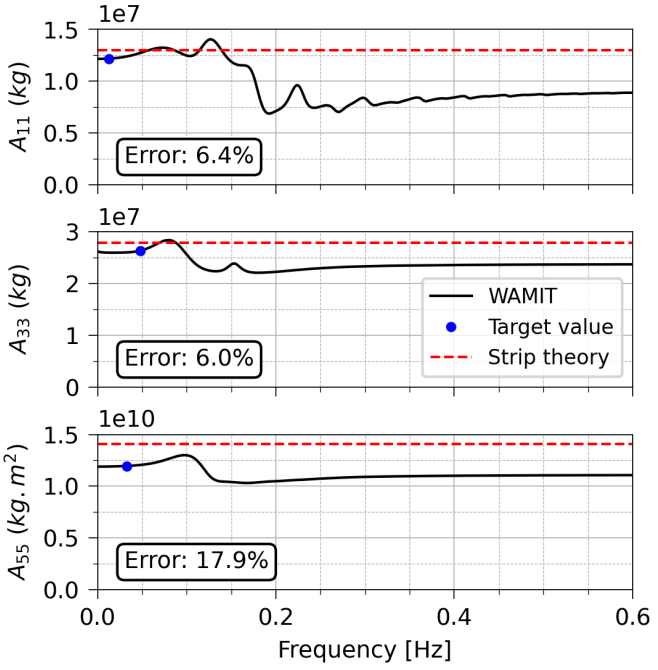

FIGURE 5: Comparison between added mass computed with WAMIT and with the strip-theory model

The resulting set of coefficients is summarized in Table 5. We prioritize the forces/moment due to our objective of validating internal loads, and that is why we deem the 18% difference in the pitch added mass (A_{55}) as acceptable.

Figure 6 also illustrates the effect of the MacCamy-Fuchs correction (MCF), evidencing the improvement for the surge force for frequencies larger than about 0.15 Hz, which corresponds to

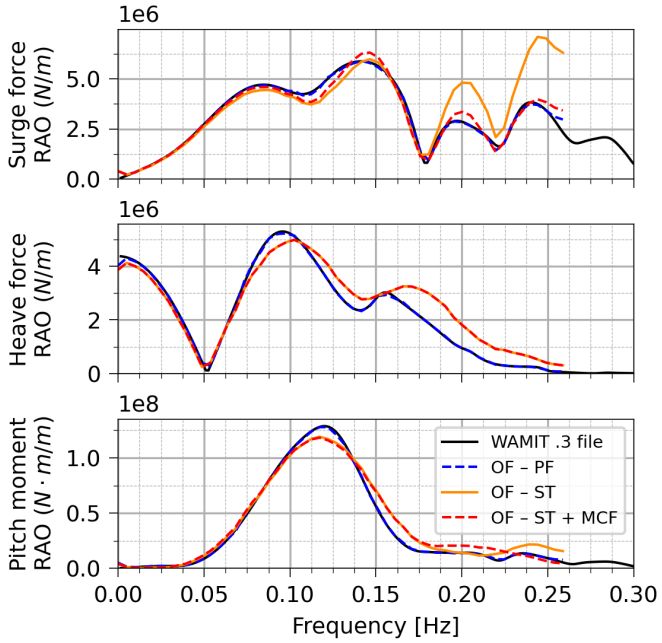

FIGURE 6: First-order wave excitation RAOs obtained with WAMIT and with OpenFAST (OF) simulations of a white-noise wave. The different OpenFAST models are based on potential-flow coefficients from WAMIT (PF), strip-theory solution (ST), or strip-theory solution with MacCamy-Fuchs correction (MCF).

TABLE 5: Main inputs for the strip-theory model

Central column	
Diameter (m)	9.85
C_a	0.85
C_D	0.40
$C_{a,end}$	0.7
$C_{D,end}$	4.0
Outer columns	
Diameter (m)	12.23
C_a	0.85
C_D	0.4 if $z < -4.0$ m $0.4 + 1.8 \cdot (z + 4)$ if $-4.0 \leq z \leq -3.5$ m 1.3 if $z > -3.5$ m
$C_{a,end}$	0.7
$C_{D,end}$	8.0
Pontoons	
Diameter (m)	10.58
C_a	0.90
C_D	1.75
Fictitious cylinders along the pontoons	
Diameter (m)	8.13
$C_{a,end}$	4.0
$C_{D,end}$	4.0

the threshold of $\lambda/D = 5$ usually adopted for the validity of the Morison equation. Because the MCF only acts on the loads transverse to the axis of the outer columns, it does not affect the heave force, and the discrepancies with respect to WAMIT are accepted as limitations of the strip-theory model. The MCF affects the pitch moment only slightly and for very short waves, because the pitch moment is mostly due to the loads on the pontoons and on the bottom of the outer columns. Because the usefulness of the MCF is already shown here, all results presented in the following sections consider the MCF unless stated otherwise.

Both the strip-theory and the hybrid approaches use the same set of transverse and axial drag coefficients, C_D and $C_{D,end}$, listed in Table 5. These coefficients were tuned based on a combination of results from previous work [15] and decay tests, which are not shown here for conciseness.

For all the simulations, we used the time series of wave elevation measured during wave calibration as input to the SeaState module.

3.3 Mooring model

We consider the fishing lines used in the experiment to be massless and without hydrodynamic loads on them. We modeled each mooring line as a linear spring using MAP++ [20] and the properties reported in [8]. We modeled the cable bundle using HydroDyn by including additional stiffness terms equal to 6.83×10^3 N/m in surge and 6.22×10^4 N/m in heave.

4. RESULTS

This section presents the comparisons between the experiments and OpenFAST simulations. For conciseness and due to the wave incidence of 0°, we focus on surge, heave, and pitch motions, and on the loads at the root of the pontoon that is aligned with the waves (axial force, vertical force, and vertical bending moment). Because the signals corresponding to the loads were demeaned in the experiments, we analyze only the dynamic part of the loads.

4.1 Regular wave

Figure 7 compares the motions obtained with the hybrid (HB) and the strip-theory (ST) OpenFAST models, both using Wheeler stretching, with the motions measured in the experiments under the action of the regular wave (period of 13.5 s and height of 10.85 m). The motions are driven mostly by first-order wave loads, as evidenced by the almost sinusoidal form of the time series and the pronounced peak of the power spectral density (PSD) at the same frequency as the incoming wave. Both models predict the standard deviation of surge motion within 5% of the experimental value. The strip-theory model performs slightly better than the hybrid model for the dynamics of the vertical DoFs: whereas the strip-theory model predicts the standard deviation of all motions within 5%, the hybrid model overpredicts the standard deviation of heave and pitch motion by 10% and 15%, respectively. Though the higher harmonics that are visible in the PSDs

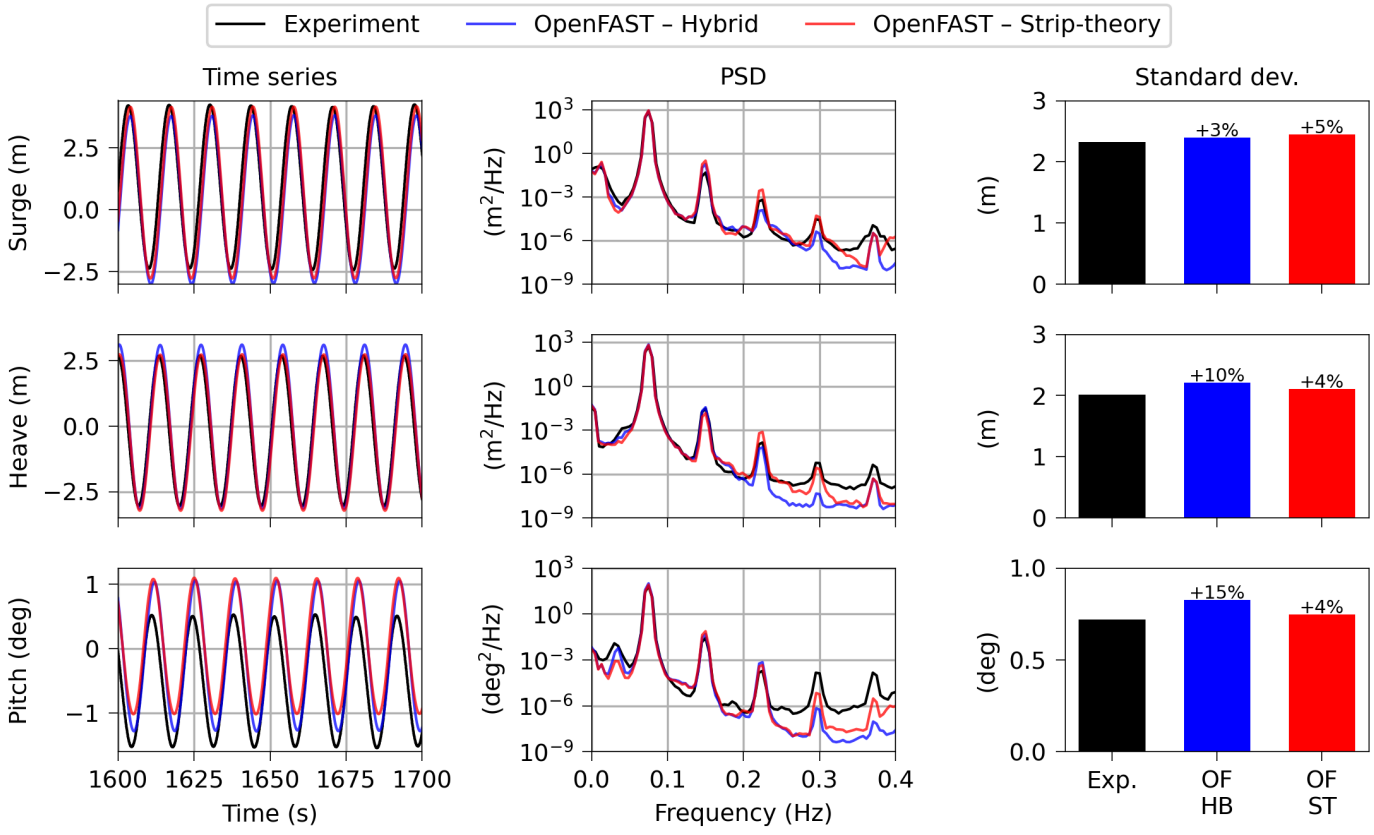

FIGURE 7: Time series (left), power spectral density (PSD), and standard deviation (right) of the motions measured in the experiments and computed with OpenFAST

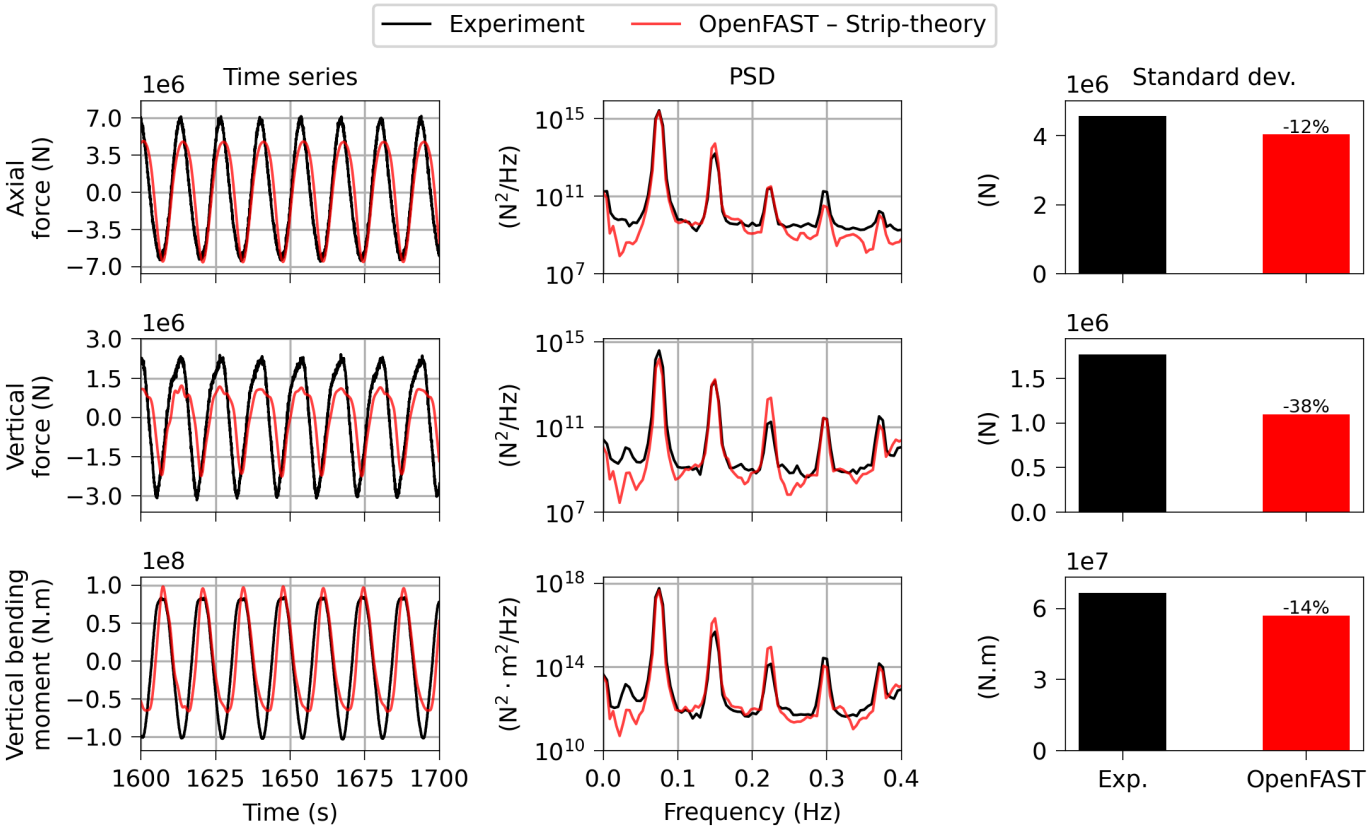

FIGURE 8: Time series (left), power spectral density (PSD), and standard deviation (right) of the loads at the root of the pontoon measured in the experiments and computed with OpenFAST

do not contribute significantly to the motions, it is interesting to note that such harmonics are well modeled by both OpenFAST models. This is a consequence of the nonlinear hydrodynamic model with the time series of wave elevation measured in the experiment as input to the numerical models.

Figure 8 presents the same analysis but for the loads at the root of the pontoon that is aligned with the waves. Only the results obtained with the strip-theory model are presented, because the loads obtained with the hybrid model are meaningless due to the hydrodynamic and hydrostatic forces/moments being lumped at a single point.

The results show a good agreement for the axial force and the vertical bending moment (which is the bending moment about the horizontal axis). Even though some qualitative differences are still visible in the time series, particularly a larger asymmetry between crests and troughs for the OpenFAST simulations than for the experiments, the standard deviation is predicted to be within 12% and 14% for the axial force and the vertical bending moment, respectively. Due to the lack of experimental uncertainty estimates, it is not possible to definitely identify the cause of the discrepancies between the experiment and the simulations.

This level of agreement is not observed for the vertical force. Unlike the motions, the time series of vertical force deviates from a sinusoidal form, thus evidencing a nonlinear behavior. This behavior is made clear by the two most prominent peaks in the PSDs: whereas the second peak in the PSD of heave motion is only about 10^{-5} of the first one, the second peak in the PSD of vertical force is about 10^{-1} of the first peak. Though both signals have troughs that are more pronounced than the crests, the vertical force computed with OpenFAST presents crests that are smoother than the ones measured in the experiments. This qualitative difference is reflected in the underprediction of 38% of the standard deviation of the vertical force by OpenFAST. It is not yet clear why the vertical force is so discrepant whereas the heave motion is well predicted. Moreover, because both the vertical force and the vertical bending moment are largely impacted by the hydrodynamic loads along the pontoons, it is surprising that the vertical bending moment is well predicted whereas the vertical force is not.

4.2 Irregular waves - IRR01

Figure 9 compares the PSD and the standard deviation of motion for the irregular wave IRR01 (T_P = 12.7 s and H_S = 8.18 m) obtained with different OpenFAST models against the experimental results. The motions present two main frequency ranges of interest: the frequencies of the incoming waves, where the motions are induced by first-order wave loads, and the natural frequency of each degree of freedom, where the motions are induced by nonlinear low-frequency wave loads. In the plots, the frequency range corresponding to the natural frequency of each DoF (see Table 1) is shaded in gray, while the one corresponding to the waves (roughly between 0.050 Hz and 0.175 Hz) is shaded

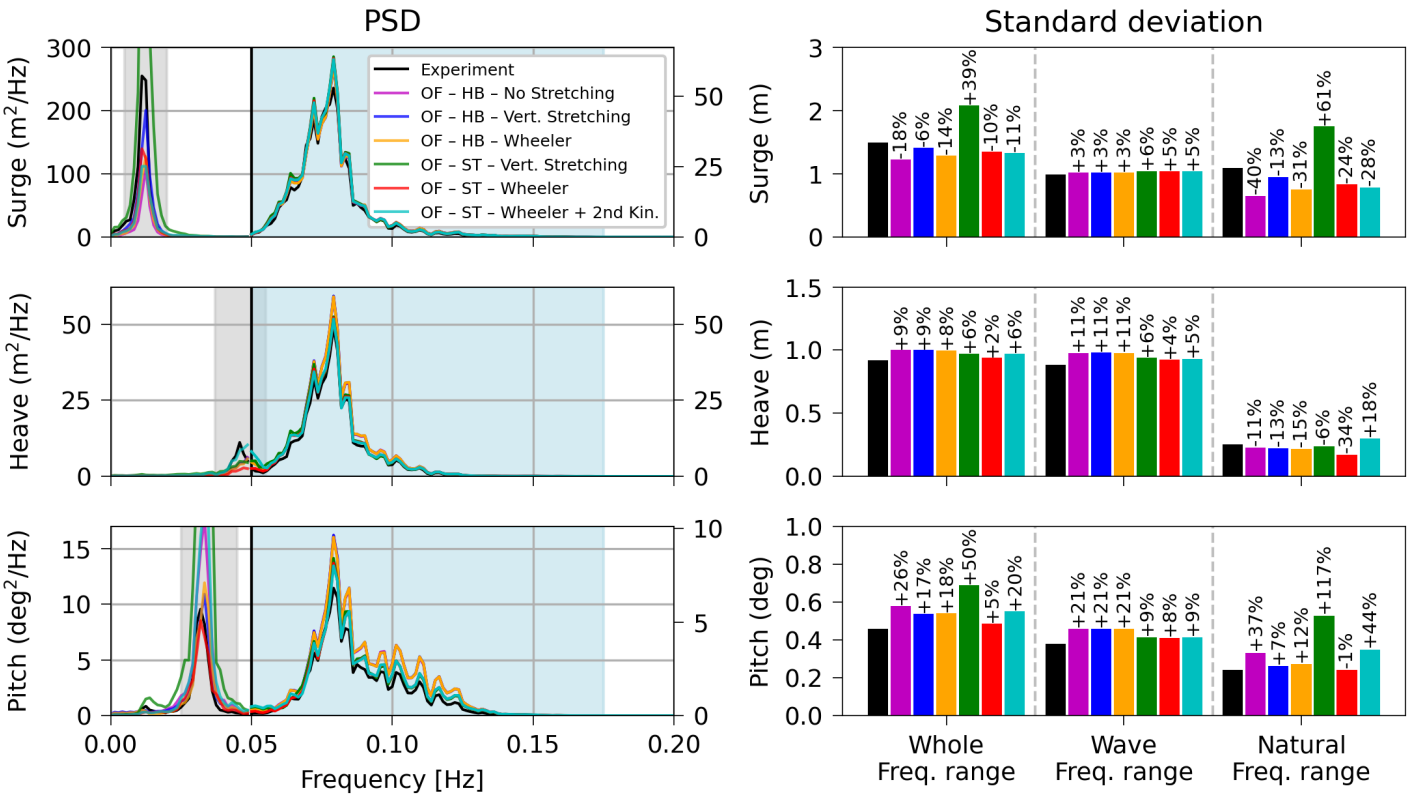

FIGURE 9: Power spectral density (PSD) of motion (left) and standard deviation (right) for each frequency range for the IRR01 wave condition. The frequency range corresponding to the natural frequency of each DoF is shaded in gray, and the one corresponding to the waves is in light blue. For better visualization, different y-axes are used for the PSDs to the left and to the right of the vertical line marking the beginning of the wave frequency range.

in light blue. Note that because the surge and pitch PSDs have large peaks at their natural frequencies, the y-axis of the PSDs corresponding to the natural frequency of motion (on the left of the vertical line shown in the plots) is different from the y-axis of the PSDs corresponding to the wave frequency (right of the vertical line) for a better visualization.

To provide a quantitative metric of the agreement between the numerical and experimental results for each of these ranges of interest, we compute the standard deviation of the motion in each range by taking the square root of the integral of the PSD in the corresponding frequency range. These two ranges exhibit a small overlap for heave, because there is still some wave energy close to its natural frequency, but we compute the integrals using the same procedure regardless of this overlap. The standard deviations are presented on the right side of Figure 9.

In the wave frequency range, the agreement follows the same pattern of the response under a regular wave discussed in Section 4.1. For surge, all models reproduce the motions at the frequency of the waves very well, with the hybrid model performing slightly better than the strip-theory model (overprediction of the standard deviation by 3% and by about 5% for the HB and ST models, respectively). For heave, the hybrid model overpredicts the standard deviation of motion by 11% and the strip-theory model overpredicts it by about 5%. The agreement is not as good for the pitch motion, with the hybrid model overpredicting the standard deviation by 21% and the strip-theory model overpredicting it by about 8% to 9%. As expected, stretching and 2nd order kinematics do not have a significant impact on the wave frequency motions.

The total standard deviation of surge, which is obtained by integrating the full frequency range, is significantly affected by the slow drift. In fact, for the surge motion measured in the experiments, the contribution of the natural frequency range is more significant than the one from the wave frequency range. It is clear from the results of the hybrid model without stretching that the utilization of full QTFs is not enough to properly reproduce the slow surge motion (underprediction of the standard deviation at the natural frequency range by 40%), which is in line with findings from previous work [15, 21]. The results of the hybrid model improve significantly with vertical stretching (underprediction of 13%), whereas Wheeler stretching provides only a small improvement (underprediction of 31%).

On the other hand, the use of vertical stretching with the strip-theory model results in a large overprediction of 61% of the standard deviation of slow surge motion, suggesting that vertical stretching of the wave acceleration overestimates the inertial part of the force—at least for this particular floating substructure and wave condition. The strip-theory model with Wheeler stretching performs better, but still presents an important underprediction of 24%. This indicates that diffraction effects (which are included

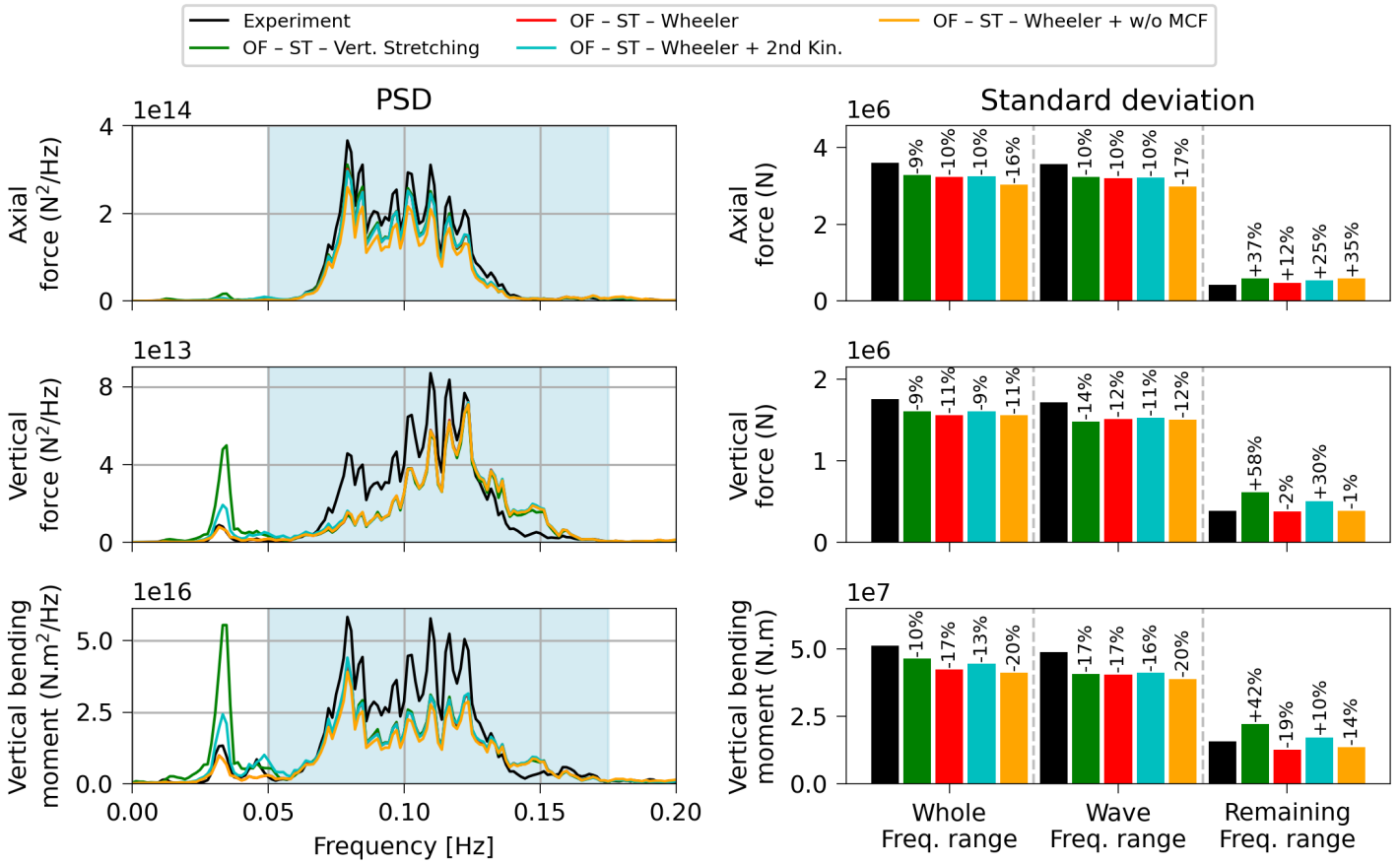

FIGURE 10: Power spectral density (PSD) of loads at the root of the pontoon aligned with the waves (left) and standard deviation (right) for each frequency range for the IRR01 wave condition. The frequency range corresponding to the waves is shaded in light blue.

in the hybrid model via the QTFs) are not completely negligible for the second-order loads in this case, which agrees with previous works that concluded that the second-order diffraction wave loads are more restrictive in terms of cylinder slenderness (ratio between the length of the incoming waves and cylinder diameter) than the first-order wave loads [22, 23]. The use of second-order wave kinematics does not impact the results significantly, further worsening the underprediction of the slow-surge motion.

Wave stretching also significantly improves the prediction of slow pitch motion, but for a different reason. Although stretching improved the slow surge response of the hybrid model by increasing the response, thus reducing the underprediction of the model when compared to using QTFs alone, the opposite happens for the slow pitch motion. The hybrid model without stretching overpredicts the standard deviation of slow pitch motion by 37%, with the vertical and Wheeler stretching models reducing this overprediction to 7% and 12%, respectively. For the strip-theory model, the use of vertical stretching leads to an overprediction of 117% of the standard deviation of slow pitch, which is even worse than for the slow surge. The use of Wheeler stretching results in an almost perfect match with respect to the experiments, with an underprediction of only 1% of the slow pitch motion. The use of second-order wave kinematics with Wheeler stretching yields a large overprediction of 44%.

The slow heave motion is practically negligible in face of the wave-frequency motion, but it merits some academic interest. Because there is still some wave energy close to the natural frequency of heave, both first- and second-order wave forces may contribute to the response. The agreement in terms of standard deviation is good in general, but that is because most numerical models predict a broader response with a smaller amplitude than the experiments. The only model that predicts a similar peak is the strip-theory model with Wheeler stretching and with second-order wave kinematics. This peak matches the natural frequency of heave measured from free decay, whereas the motions measured in the experiment present a peak slightly shifted to the left (0.046 Hz). It is also interesting to note that the strip-theory model with Wheeler stretching but without second-order wave kinematics presents a worse underprediction of the slow heave compared to the other models. This is related to how Wheeler stretching modifies the kinematics of the whole fluid domain, as opposed to the vertical wave stretching that only modifies wave kinematics in the wave trough/crest.

Figure 10 presents a similar analysis for the loads at the root of the pontoon that is aligned with the waves. In this case there is not just a single resonant frequency of interest for each of the loads, so we compute the standard deviation considering the wave-frequency range (shaded in light blue) and outside this

range. This approach is enough to weigh the relevance of the wave-frequency loads compared to the nonlinear loads. Only the results obtained with the strip-theory model are presented, because the loads obtained with the hybrid model are meaningless due to the hydrodynamic and hydrostatic forces/moments being lumped at a single point.

For the axial force, all models with the MCF present a very good agreement with the experiments, predicting the standard deviation within 10%. Though we omitted the results without the MCF in Figure 9 because it barely impacts the motions for this wave condition, it is clear from Figure 10 that the MCF is important for the loads, because the model without it performs significantly worse than the others (underprediction of 17%). The axial force is dominated by the wave-frequency range, so the use of stretching and second-order wave kinematics does not impact the results significantly. Nonetheless, just like for the slow-surge and slow-pitch motions, the model with Wheeler stretching and without second-order wave kinematics performs better than the others outside the wave-frequency range.

Though the standard deviation of the vertical force is fairly predicted by the OpenFAST models (underprediction of about 9% to 11%), this agreement is misleading. The PSD of the vertical force shows an important underestimation between roughly 0.07 Hz and 0.12 Hz, which is consistent with the underprediction of the vertical force observed for the regular wave. This underprediction is compensated to some extent by an overestimation around 0.15 Hz. Like the axial force, the vertical force acts mostly at the wave-frequency range, with only a small contribution at the natural frequency of pitch outside this range. The nonlinear force is better reproduced by the model with Wheeler stretching and without second-order wave kinematics, the same model that better reproduces the slow-pitch motion. The discrepancy in the vertical force is observed neither in the motions nor the vertical bending moment, and we do not know yet what is causing it.

The agreement of the vertical bending moment is not as good as for the axial force, but it is still acceptable. The standard deviation at the frequency of the waves is predicted within 17% by all models with the MCF, while the model without the MCF presents an underprediction of 20%. There is a small contribution near the natural frequencies of pitch and heave to the vertical bending moment, with the simulations presenting the same behavior discussed for the motions (overprediction at the natural frequency of pitch with the vertical stretching model; only the model with second-order wave kinematics presents the peak at the natural frequency of heave). One should be careful, however, because the overprediction of the loads outside the wave-frequency range observed for some models may hide the underprediction of the loads at the wave-frequency range when looking at the total standard deviation.

The strip-theory model with the MCF, with Wheeler stretching, and without second-order wave kinematics presents overall adherence with the experiment for both motions and loads, despite some disagreement in the vertical force that remains unexplained.

4.3 Irregular waves - IRR02

Figure 11 shows the PSD and the standard deviation of motion for the IRR02 condition (T_P = 8.9 s and H_S = 3.20 m) obtained with OpenFAST and from the experimental measurements.

Though the IRR02 condition is more challenging to the strip-theory model due to the shorter length of its wave components compared to IRR01, the numerical simulations show a good adherence with the experimental results in the wave frequency region. Both the strip-theory and the hybrid models perform equally well for the surge motion at the frequency of the incoming waves (overestimation of about 5%). The strip-theory model also performs slightly better in heave (overestimation of 4%) than the hybrid model (overestimation of 10%). Like the IRR01 and REG waves, the strip-theory model performs better than the hybrid model for the pitch motion, overestimating the standard deviation by about 10%, whereas the hybrid model presents an overestimation of 25%.

For the slow-surge motion, the hybrid model with vertical stretching provides a very good match with the experiments, with an underestimation of only 6% of the standard deviation. The hybrid model with Wheeler stretching provides a significantly worse prediction, with an underestimation of 21%. The better performance of the hybrid model without stretching (thus with full QTFs only) compared to the IRR01 condition shows that diffraction effects are more important for this wave condition, which is expected due to the shorter wave components (more wave scattering) and lower wave height (reduction of the importance of wave stretching). Consequently, the strip-theory model is incapable of properly reproducing the slow-surge motion regardless of the stretching model or the use of second-order wave kinematics (underprediction of more than 45%).

The heave motion shows a more pronounced response at the natural frequency than the one observed for the IRR01 condition. This peak is mostly induced by the second-order wave potential, which has a slower depth decay than the other second-order force components, as evidenced by the response of the strip-theory model with second-order wave kinematics.

The slow-pitch motion is overestimated by all numerical models, especially by the strip-theory model with Wheeler stretching and second-order wave kinematics. Though the strip-theory model with vertical stretching performed better for both the slow-surge and slow-pitch motions, this is probably due to compensating the lack of diffraction effects rather than to the vertical stretching itself properly reproducing the forces acting on the structure. The slow-pitch motion predicted by the hybrid model is insensitive to the stretching model, suggesting that the slow-pitch motion is mostly due to the loads on the pontoons.

Figure 12 presents the PSDs and the standard deviation of the loads at the root of the pontoon that is aligned with the waves. Once again, the loads act mostly at the wave-frequency range, and we discuss only the loads obtained with the strip-theory models.

The numerical models match very well the axial force, with the MCF slightly improving the results (improvement from an underestimation of 14% to about 12%).

The strip-theory model is capable of properly predicting the vertical force (underprediction of about 5%), because this wave

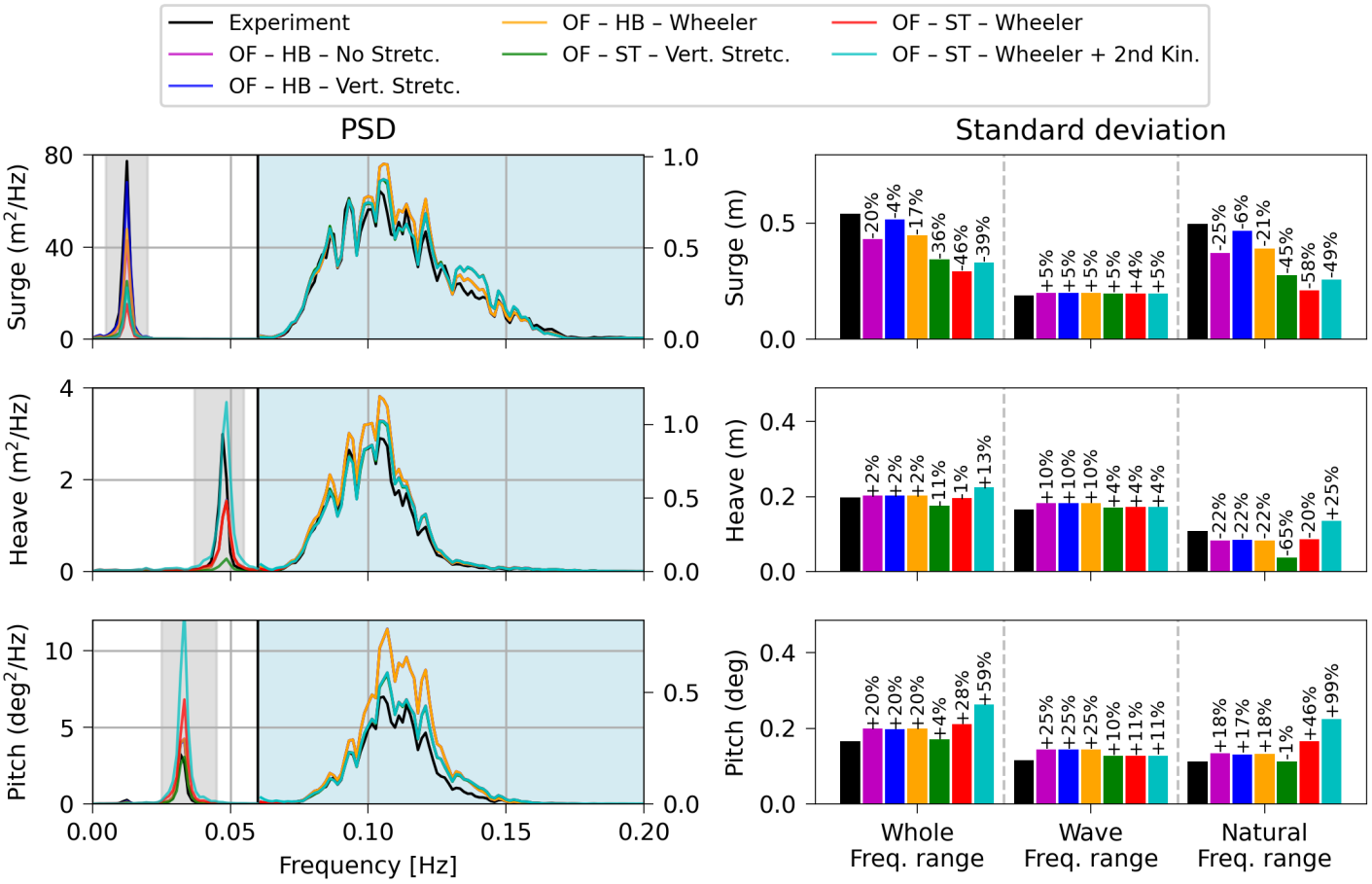

FIGURE 11: Power spectral density (PSD) of motion (left) and standard deviation (right) for each frequency range for the IRR02 wave condition. The frequency range corresponding to the natural frequency of each DoF is shaded in gray, and the one corresponding to the waves is in light blue. For better visualization, different y-axes are used for the PSDs to the left and to the right of the vertical line marking the beginning of the wave frequency range.

condition does not contain significant wave energy at the frequencies that presented an underprediction of the vertical load observed for the IRR01 and REG. Again, there is a practically negligible contribution from the natural frequency of pitch to the vertical force, with the differences in the force being closely related to the ones observed for the slow pitch motion.

The models do not perform as well for the vertical bending moment, presenting an underprediction of about 20% of the standard deviation. One important qualitative difference between the numerical and experimental results is the presence of a peak around 0.16 Hz that is not observed in the numerical simulations. This frequency corresponds, roughly, to a wavelength that is equal to the distance between the center of the central column and the center of the outer column aligned with the wave direction, so that the floating substructure is sagging/hogging. This situation corresponds to a peak in the heave force acting on the whole floating substructure, which is shown in Figure 6 to be displaced by the strip-theory model compared to the hybrid model, suggesting that this difference may be due to wave diffraction effects. This discrepancy could also be due to couplings in the measurements of the 6-DoF load cell that are not included in the numerical models. It is worth mentioning that the visual differences presented by the PSDs are not a fair measure of the agreement between the numerical and experimental results, because the PSDs magnify the differences because they are proportional to the square of the amplitudes.

5. CONCLUSION

This article presented the validation of the local structural load modeling capability in OpenFAST for floating substructures based on data from the FOCAL experimental campaign. For conciseness, we focused on wave-only conditions. Due to the wave incidence of 0°, the comparisons considered the surge, heave, and pitch motions of the FOWT and the loads at the root of the pontoon that is aligned with the waves (axial force, vertical force, and vertical bending moment).

To model the distributed hydrodynamic and hydrostatic loads along the floating substructure, we adopted a strip-theory approach based on the Morison equation. To assess the performance of the strip-theory model, we also did simulations with a hybrid model that uses a combination of the quadratic drag from the Morison equation with radiation/diffraction loads obtained from

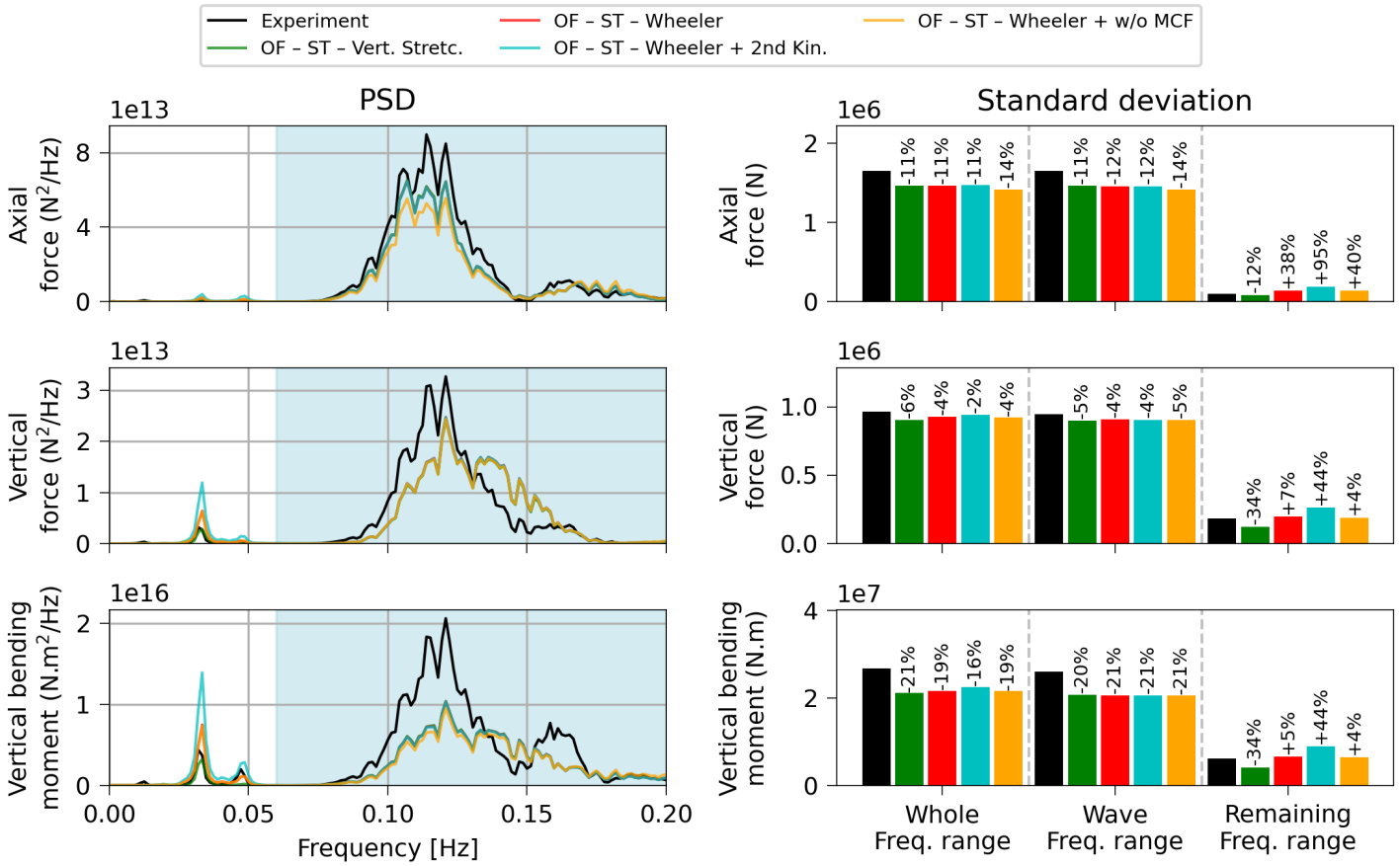

FIGURE 12: Power spectral density (PSD) of loads at the root of the pontoon aligned with the waves (left) and standard deviation (right) for each frequency range for the IRR02 wave condition. The frequency range corresponding to the waves is shaded in light blue.

frequency-dependent coefficients precomputed with WAMIT—including full quadratic transfer functions (QTFs). This hybrid model, however, is only able to model the rigid-body motions of the structure, because the radiation/diffraction loads are lumped at a single point of the structure. We also discussed the impact of different hydrodynamic modeling options—wave stretching, MacCamy-Fuchs correction (MCF), and second-order wave kinematics—on both motions and loads.

The comparisons showed that the MCF improves the prediction of the transversal loads on the outer columns in short waves, thus improving the surge force and the axial force measured in the load cell in the wave-frequency range. Concerning wave stretching, the vertical wave stretching approach performed very well with the hybrid model, but led to a large overestimation of the slow-surge and slow-pitch motions when employed with the strip-theory model. This indicates that vertical stretching of the wave acceleration overestimates the inertial part of the force—at least for this particular floating substructure and the wave conditions considered. Second-order wave kinematics did not improve the results significantly, except for a better prediction of the slow-heave motion. The slow heave, however, is of limited relevance in the presence of the response at the frequency of the incoming waves.

The loads at the root of the pontoon were dominated by the wave-frequency range, with negligible contributions at the natural frequencies of motion. We obtained good results for the axial loads, with an agreement within 5% for the REG and IRR01 wave conditions and within 12% for IRR02. For the vertical force, the simulations presented a significant underprediction for frequencies between 0.07 Hz and 0.12 Hz that is reflected in an underprediction of the standard deviation for the IRR01 and REG waves (38% and 12%, respectively), but not for the IRR02 wave (underprediction of 4%). This is because the IRR02 wave does not contain significant wave energy at those frequencies. The vertical bending moment presents a fair adherence with the experimental results (underprediction of 14% for the REG wave, 17% for IRR01, and 21% for IRR02).

Though it is not possible to definitely identify the cause of the discrepancies between the experiment and the simulations, OpenFAST shows promise in predicting the motion and structural loads of floating substructures.

ACKNOWLEDGMENTS

This work was authored by the National Renewable Energy Laboratory, operated by the Alliance for Sustainable Energy, LLC, for the U.S. Department of Energy (DOE) under Contract No. DE-AC36-08GO28308. Funding provided by the U.S. Department of Energy Office of Energy Efficiency and Renewable

Energy Wind Energy Technologies Office. The views expressed in the article do not necessarily represent the views of the DOE or the U.S. Government. The U.S. Government retains and the publisher, by accepting the article for publication, acknowledges that the U.S. Government retains a nonexclusive, paid-up, irrevocable, worldwide license to publish or reproduce the published form of this work, or allow others to do so, for U.S. Government purposes.

REFERENCES

[1] GWEC. "Global Wind Report." (2023).

[2] Jonkman, B., Mudafort, R., Platt, A., Branlard, E., Sprague, M., Ross, H., Jonkman, J., Hayman, G., Hall, M., Slaughter, D., Vijayakumar, G., Buhl, M., Russel, A., Bortolotti, P., Ananthan, S., Rood, J., Damiani, R., Mendoza, N., Long, H., Schunemann, P., Sharma, A., Shaler, K., Housner, S., Sakievich, P., Bendl, K., Carmo, L., Quon, E. and Phillips, M. "OpenFAST/openfast: v3.5.0." (2023). DOI 10.5281/zenodo.7942867.

[3] Son, D., Pinguet, R. and Roddier, D. "Global sizing of the WindFloat for a 10 MW generic wind turbine." *International Offshore Wind Technical Conference*, Vol. 51975: p. V001T01A035. 2018. ASME. DOI 10.1115/IOWTC2018-1104.

[4] Lizarraga-Saenz, I., Artal-García, J., Martín-San-Román, R., Vittori, F. and Azcona-Armendáriz, J. "Study of the influence of met-ocean data in fatigue loads calculations of a floating offshore wind turbine." *Journal of Physics: Conference Series*, Vol. 2265. 4: p. 042014. 2022. IOP Publishing. DOI 10.1088/1742-6596/2265/4/042014.

[5] Bergua, R., Robertson, A., Jonkman, J., Platt, A., Page, A., Qvist, J., Amet, E., Cai, Z., Han, H., Beardsell, A., Shi, W., Galván, J., Bachynski-Polić, E., McKinnon, G., Harnois, V., Bonnet, P., Suja-Thauvin, L., Hansen, A., Alonso, I., Aristondo, A., Battistella, T., Guanche, R., Schünemann, P., Pham, T., Trubat, P., Alarcón, D., Haudin, F., Nguyen, M. and Goveas, A. "OC6 Phase II: Integration and verification of a new soil–structure interaction model for offshore wind design." *Wind Energy* Vol. 25 No. 5 (2022): pp. 793–810. DOI 10.1002/we.2698.

[6] Jonkman, J., Branlard, E., Hall, M., Hayman, G., Platt, A. and Robertson, A. "Implementation of substructure flexibility and member-level load capabilities for floating offshore wind turbines in OpenFAST." Technical Report No. TP-5000-76822. National Renewable Energy Laboratory, Golden, CO, USA. 2020.

[7] Thomsen, J., Bergua, R., Jonkman, J., Robertson, A., Mendoza, N., Brown, C., Galinos, C. and Stiesdal, H. "Modeling the TetraSpar floating offshore wind turbine foundation as a flexible structure in OrcaFlex and OpenFAST." *Energies* Vol. 14 No. 23 (2021): p. 7866. DOI 10.3390/en14237866.

[8] Lenfest, E. and Fowler, M. "Floating offshore wind controls advanced laboratory (FOCAL) experimental program - Campaign 4." Technical Report No. 23-57-1183. University of Maine's Advanced Structures and Composites Center, Orono, ME, USA. 2023.

[9] Wang, L., Bergua, R., Robertson, A., Jonkman, J., Ngo, T., Das, T., Sarker, D., Flavia, F., Harries, R., Fowler, M., Lenfest, E., Muro, J., Burlion, L. and Bilgen, O. "Experimental validation of models of a hull-based tuned mass damper system for a semisubmersible floating offshore wind turbine platform." *Journal of Physics: Conference Series*, Vol. 2626. 1: p. 012067. 2023. IOP Publishing. DOI 10.1088/1742-6596/2626/1/012067.

[10] Fowler, M., Lenfest, E., Viselli, A., Goupee, A., Kimball, R., Bergua, R., Wang, L., Zalkind, D., Wright, A. and Robertson, A. "Wind/wave testing of a 1:70-scale performance-matched model of the IEA wind 15 MW reference wind turbine with real-time ROSCO control and floating feedback." *Machines* Vol. 11 No. 9 (2023): p. 865. DOI 10.3390/machines11090865.

[11] Fowler, M., Lenfest, E., Viselli, A., Goupee, A., Kimball, R., Zalkind, D., Wright, A., Bergua, R., Wang, L. and Robertson, A. "1:70-Scale model testing of the Reference OpenSource Controller (ROSCO) on the IEA-wind 15MW reference wind turbine including floating feedback." *International Ocean and Polar Engineering Conference*: pp. ISOPE–I. 2023. ISOPE.

[12] Wang, L., Bergua, R., Robertson, A., Wright, A., Zalkind, D., Fowler, M., Lenfest, E., Viselli, A., Goupee, A. and Kimball, R. "Experimental investigation of advanced turbine control strategies and load-mitigation measures with a model-scale floating offshore wind turbine system." *Applied Energy* Vol. 355 (2024). DOI 10.1016/j.apenergy.2023.122343.

[13] Gaertner, E., Rinker, J., Sethuraman, L., Zahle, F., Anderson, B., Barter, G., Abbas, N., Meng, F., Bortolotti, P., Skrzypinski, W., Scott, G., Feil, R., Bredmose, H., Dykes, K., Shields, M., Allen, C. and Viselli, A. "Definition of the IEA Wind 15-Megawatt Offshore Reference Wind Turbine." (2020).

[14] Allen, C., Viscelli, A., Dagher, H., Goupee, A., Gaertner, E., Abbas, N., Hall, M. and Barter, G. "Definition of the UMaine VolturnUS-S reference platform developed for the IEA Wind 15-Megawatt offshore reference wind turbine." Technical report no. National Renewable Energy Lab.(NREL), Golden, CO, USA; Univ. of Maine, Orono, ME, USA. 2020.

[15] Wang, L., Robertson, A., Jonkman, J. and Yu, Y. "OC6 phase I: Improvements to the OpenFAST predictions of nonlinear, low-frequency responses of a floating offshore wind turbine platform." *Renewable Energy* Vol. 187 (2022): pp. 282–301. DOI 10.1016/j.renene.2022.01.053.

[16] Wang, L., Jonkman, J., Hayman, G., Platt, A., Jonkman, B. and Robertson, A. "Recent hydrodynamic modeling enhancements in OpenFAST." *International Offshore Wind Technical Conference*, Vol. 86618: p. V001T01A004. 2022. American Society of Mechanical Engineers. DOI 10.1115/IOWTC2022-98094.

[17] WAMIT, Inc. *WAMIT User Manual - Version 7.4*. Chestnut Hill, MA, USA (2020).

[18] Bergua, R., Wiley, W., Robertson, A., Jonkman, J., Brun, C., Pineau, J., Qian, Q., Maoshi, W., Beardsell, A., Cutler, J.,

Pierella, F., Hanse, A., Shi, W., Fu, J., Hu, L., Vlachogiannis, P., Peyrard, C., Wright, C., Friel, D., Hanssen-Bauer, Ø., dos Santos, C., Frickel, E., Islam, H., Koop, A., Hu, Z., Yang, J., Quideau, T., Harnois, V., Shaler, K., Netzband, S., Alarcón, D., Trubaut, P., Connolly, A., Leen, S. and Conway, O. "OC6 Project Phase IV: Validation of numerical models for novel floating offshore wind support structures." *Wind Energy Science Discussions* Vol. 2023 (2023): pp. 1–36. DOI 10.5194/wes-2023-103.

[19] MacCamy, R. and Fuchs, R. *Wave forces on piles: a diffraction theory*. 69, US Beach Erosion Board (1954).

[20] Masciola, M., Jonkman, J. and Robertson, A. "Implementation of a multisegmented, quasi-static cable model." *International Ocean and Polar Engineering Conference*. 2013. ISOPE.

[21] Robertson, A., Wendt, F., Jonkman, J., Popko, W., Dagher, H., Gueydon, S., Qvist, J., Vittori, F., Azcona, José, Uzunoglu, E., Soares, C., Harries, R., Yde, A., Galinos, C., Hermans, K., de Vaal, J., Bozonnet, P., Bouy, L., Bayati, I., Bergua, R., Galvan, J., Mendikoa, I., Sanchez, C., Shin, H., Oh, S., Molins, C. and Debruyne, Y. "OC5 Project Phase II: Validation of Global Loads of the DeepCwind Floating Semisubmersible Wind Turbine." *Energy Procedia* Vol. 137 (2017): pp. 38 – 57. DOI 10.1016/j.egypro.2017.10.333. 14th Deep Sea Offshore Wind R&D Conference, EERA DeepWind.

[22] Carmo, L. and Simos, A. "On the complementarity of the slender-body and Newman's approximations for difference-frequency second-order wave loads on slender cylinders." *Ocean Engineering* Vol. 259 (2022): p. 111905. DOI 10.1016/j.oceaneng.2022.111905.

[23] Carmo, L., Simos, A. and de Mello, P. "A second-order slender-body approach for computing wave induced forces with application to a simplified semi-submersible FOWT model." *Ocean Engineering* Vol. 285 (2023): p. 115410. DOI 10.1016/j.oceaneng.2023.115410.